


High-temperature mass spectrometric study and modeling of thermodynamic properties in the $\text{La}_2\text{O}_3\text{-TiO}_2$ system

Valentina L. Stolyarova^{a,b,*} , Andrey L. Shilov^a, Viktor A. Vorozhtcov^a, Sergey I. Lopatin^a, Anna V. Fedorova^{a,b}

^a Institute of Silicate Chemistry of Russian Academy of Sciences, Makarova Emb., 2, St. Petersburg 199034, Russia

^b Saint Petersburg State University, Universitetskaya Emb. 7/9, St. Petersburg 199034, Russia

ARTICLE INFO

Keywords:

$\text{La}_2\text{O}_3\text{-TiO}_2$ system
Knudsen effusion mass spectrometry
Vaporization
Modeling
Thermodynamics

ABSTRACT

The vapor composition over two samples of the $\text{La}_2\text{O}_3\text{-TiO}_2$ system containing 50 and 90 mole % TiO_2 was explored by the high-temperature Knudsen effusion mass spectrometric method. TiO_2 , TiO , and LaO species were identified in the vapor. From the measured partial pressures of the vapor species, the TiO_2 activity as a function of composition was determined at the temperatures of 2290 K and 2475 K. As a result of modeling within the generalized lattice theory of associated solutions, the La_2O_3 activity was determined. The obtained component activities and the excess Gibbs energy indicate strong negative deviations from the ideal behavior, which are illustrated by the calculated concentration dependence of the relative number of mixed bonds in the system under study.

1. Introduction

Materials based on high-entropy oxides, carbides, and oxycarbides find ever-growing application in various fields of modern technology [1–4], stimulating further research into this direction for solving still more complicated technological problems [5–7]. The unique combination of physicochemical properties of these materials enables their application in such areas as preparation of ultra-high-temperature ceramics including improved high temperature coatings [8–10], oxygen storage [11], separation of oxygen from the gaseous mixtures [12], chemical looping processes [11,13], and obtaining syngas using the oxidation of methane [14].

The electrochemical and photochemical properties of high-entropy oxides with the perovskite structure are of special interest in many aspects. They can be used in perovskite photocells, in which the band gap of TiO_2 or ZrO_2 can be changed by introducing a large number of other oxides [15]. High entropy oxide $[(\text{Bi},\text{Na})_{0.2}(\text{La},\text{Li})_{0.2}(\text{Ce},\text{K})_{0.2}\text{Ca}_{0.2}\text{Sr}_{0.2}]\text{TiO}_3$ was considered as anode material for lithium-ion batteries [16]. Oxycarbide phases exhibit greater chemical inertness with respect to oxidation at high temperatures compared to the corresponding carbides [3,17,18], and therefore high-entropy oxycarbides may be considered as the optimal and most promising candidates for creating materials of

higher refractoriness. But currently, there is practically no information on the high-temperature description of the physicochemical processes taking place even in materials based on the most studied class of compounds, which are high-entropy oxides. This significantly restricts the ability to predict, develop, synthesize, and exploit these materials.

Knudsen effusion mass spectrometry (KEMS) [19,20] is firmly established as one of the most informative methods for determination of the thermodynamic properties of oxides and many other substances at the temperatures above 1000 K. It provides most detailed information on the composition of the vapor phase and partial pressures of the vapor species over the vaporized samples of multicomponent systems essential for planning the synthesis procedures and evaluation of the product performance [21,22]. The potential of the KEMS method to study the thermodynamic properties of highly refractory systems has repeatedly been demonstrated earlier [23–25].

The objective of the present study is the KEMS investigation of the vaporization processes and thermodynamic properties of the samples in the $\text{La}_2\text{O}_3\text{-TiO}_2$ system, which is a constituent part of certain multicomponent high-entropy oxides. Only the data related to the partial pressures over pure oxides and their vaporization enthalpies have been found in the literature: vaporization of La_2O_3 proceeds with the formation of LaO , O , and negligible amounts of La in the vapor [26,27]; the

* Corresponding author at: Saint Petersburg State University, Universitetskaya nab., 7/9, St. Petersburg 199034, Russia.

E-mail addresses: v.stolyarova@spbu.ru (V.L. Stolyarova), naskalinen@mail.ru (A.L. Shilov), v.vorozhtcov@rambler.ru (V.A. Vorozhtcov), s.lopatin@spbu.ru (S.I. Lopatin), a.v.fedorova@spbu.ru (A.V. Fedorova).

<https://doi.org/10.1016/j.ctta.2025.100164>

Received 31 July 2024; Received in revised form 22 December 2024; Accepted 8 January 2025

Available online 9 January 2025

2667-3126/© 2025 The Authors. Published by Elsevier B.V. CCBYLICENSE This is an open access article under the CC BY-NC license (<http://creativecommons.org/licenses/by-nc/4.0/>).

main vapor species over pure TiO₂ are TiO₂, TiO, and O [28,29]. The thermodynamic data for the binary La₂O₃-TiO₂ system obtained in the present study by the KEMS method will be used later for characterization and modeling of multicomponent oxide systems Sr-La-Ti-Hf-Fe-O and Sr-La-Ti-Hf-Fe-O-C.

2. Experimental

2.1. Samples synthesis

The samples in the La₂O₃-TiO₂ system were prepared by conventional solid-state synthesis. The reagents were ultra high purity La₂O₃ (99.995 %, TU 48-4-523-90 specifications, Russia) and TiO₂ (99.999 %, TU 6-09-3811-79 specifications, Russia). The required amounts of lanthanum oxide and titanium oxide weighed on OHAUS analytical balance with the accuracy of ±0.0001 g were homogenized for 1 hour in an agate mortar in ethanol medium. Next, the blend was shaped into pellets in a plexiglass pellet die. The pellets were calcined for 30 h at the temperature of 1573 K to guarantee the stability of the phase composition. The calcination was carried out at the atmospheric pressure in the high-temperature Nabertherm HTC 03/15 (Germany) furnace equipped with B180 controller.

Two samples were prepared with the composition 10 mole % La₂O₃ and 90 mole % TiO₂ (sample N 1) and with the composition 50 mole % La₂O₃ and 50 mole % TiO₂ (sample N 2). Phase analysis of the samples at room temperature indicated that the most abundant phase in sample N 1 is polymorph rutile modification of TiO₂, with lesser admixtures of monoclinic La₂Ti₂O₇ and orthorhombic La₄Ti₉O₂₄, Fig. S1 in Supporting information. In sample N 2, XRD patterns revealed two phases: lanthanum titanate La₂TiO₅ and lanthanum dititanate La₂Ti₂O₇, as shown in Fig. S2.

Elemental composition of the synthesized samples was determined by X-ray fluorescence analysis. The results presented in Table 1 indicate that average deviation of compositions by analysis from the compositions by synthesis is within 7 %. Only the characteristic peaks of lanthanum, titanium, and rhodium were discovered in the energy-dispersive spectrum of the La₂O₃-TiO₂ sample. The characteristic peaks of rhodium, which were also present in the spectrum, originated from the anode material of the spectrometer used for the analysis.

A more detailed account of the instrumentation and the results of analysis are given in the Supporting information.

2.2. Knudsen effusion mass spectrometry

The vaporization processes and thermodynamic properties of two samples in the La₂O₃-TiO₂ system containing 90 and 50 mole % TiO₂ (samples NN 1 and 2) were investigated by the high-temperature Knudsen effusion mass spectrometric method. The data were obtained on a mass spectrometer (the MS-1301 model, Russia) using 30 V ionization voltage. The samples were vaporized from a tungsten twin effusion cell heated by electron bombardment. One chamber of the twin cell was charged with the sample under study, the other one, used as a reference, was charged with pure TiO₂, thus implementing the differential mass spectrometry technique. The temperature was measured with an optical pyrometer (model EOP-66, Ukraine). The pyrometer is checked regularly in D.I. Mendeleev Institute for Metrology.

The vapor pressure of CaF₂ served as a standard [30] for a calibration

Table 1
X-ray fluorescence analysis of the samples in the La₂O₃-TiO₂ system.

La ₂ O ₃ :TiO ₂ , batch concentrations, mole %	Concentrations according to XRF analysis, mole %	
	La ₂ O ₃	TiO ₂
50:50	52±6	50±3
10:90	8 ± 4	92±5

of the mass spectrometer. To carry out the calibration, in separate experiments without the samples of the La₂O₃-TiO₂ system, the CaF₂ vapor pressure was measured over CaF₂, vaporizing from the effusion cell, by the complete isothermal vaporization method. The determined CaF₂ pressure value was compared to the reference book data [30]. The discrepancy between the experimental and reference values of the CaF₂ vapor pressure over CaF₂ was attributed to a difference of the real vaporization temperature from the temperature measurement by the optical pyrometer, which allowed the temperature correction factor to be obtained. In subsequent experiments with the samples under study, the obtained correction factor was added to the optical pyrometer measurements to determine the temperatures of the sample vaporization.

It should be mentioned that the temperature correction factor is related not to the error of the pyrometer itself but to two main accompanying phenomena. The first phenomenon is a change in the transmittance of the pyrometric glass, through which the temperature of the effusion cell is detected. As time passes, substances under study are deposited onto the pyrometric glass, and this affects the correctness of the temperature determination. The second phenomenon is related to the fact that temperature is detected in the area of the pyrometric channel of the effusion cell. But partial pressures of vapor species in the cell are influenced by the temperature of the coldest part in the cell. The temperature difference between the pyrometric channel and the coldest part in the cell can be up to ten kelvins. This phenomenon is also taken into account by the temperature correction factor obtained in the calibration procedure.

The CaF₂ partial pressure over calcium fluoride was obtained by the Hertz-Knudsen equation, Eq. (1):

$$p_i = \frac{q_i}{tsL} \sqrt{\frac{2\pi RT}{M_i}}, \quad (1)$$

where p_i is the partial pressure of the vapor species i , q_i is the mass of the sample vaporized as the vapor species i , s is the area of vaporization surface, which is assumed to be equal to the area of the effusion orifice, t is the vaporization time, L is the Clausing coefficient, π is the pi number, R is the universal gas constant, T is the vaporization temperature, M_i is the molar mass of the vapor species i .

In the calibration procedure, $i = \text{CaF}_2$, the mass of the sample q_i was 3.7 mg, the effusion orifice area s was 0.31 mm², the Clausing coefficient was 0.9, the vaporization temperature T was measured by the optical pyrometer as 1551 K. The time t of the complete vaporization of this mass of CaF₂ at 1551 K was found as 300 min. Thus, according to Eq. (1), the value of the CaF₂ partial pressure over calcium fluoride obtained by the complete isothermal vaporization method in this study was 0.75 Pa at 1551 K. According to the literature data [30], the partial pressure of CaF₂ over calcium fluoride at 1551 K is 0.92 Pa. This leads to the temperature correction factor of -10 K. It means that the real temperature of the CaF₂ complete vaporization in the experiment was 1541 K rather than 1551 K obtained by the optical pyrometer. This temperature correction factor was applied to all temperature measurements by the optical pyrometer in the subsequent experiments with the samples of the La₂O₃-TiO₂ system.

The partial pressures of the vapor species over the samples in the La₂O₃-TiO₂ system were determined by the ion current comparison method, Eq. (2):

$$p_i = p_{st} \frac{I_i T_i \sigma_{st} \gamma_{st}}{I_{st} T_{st} \sigma_i \gamma_i}, \quad (2)$$

where I_i is the ion current, σ_i is the ionization cross section, γ_i is the conversion coefficient of the secondary electron multiplier specified as $1/\sqrt{M_i}$. Indices i and st denote the sample and the standard. In the present study, silver was chosen as the internal vapor pressure standard since silver interacts neither with the sample nor with the material of the

Knudsen cell and the Ag vapor pressure over silver was recommended by IUPAC [31]. Unfortunately, pure TiO₂, which would eliminate the ratios of ionization cross-sections and coefficients of the secondary electron multiplier in Eq. (2), could not be used as a vapor pressure standard since TiO₂ is not a congruently vaporizing substance and the temperature dependences of the partial pressures of the vapor species over it have not been reliably determined and accepted yet. So, calculation of partial pressures relied on the method of cross-sections evaluation recommended by Drowart et al. [19], making the assumption that $\sigma(\text{MO})/\sigma(\text{M}) = 0.65$ and $\sigma(\text{MO}_2)/\sigma(\text{MO}) = 0.50$. The ionization cross-sections of atomic titanium and lanthanum were taken from Mann [32]. The partial pressure of atomic oxygen could not be measured directly because of the high background level at $m/z = 16$ and had to be evaluated by Eq. (3) [33] derived as presented earlier by Kablov et al. [34]:

$$p(\text{O}) = p(\text{TiO})\sqrt{\frac{M(\text{O})}{M(\text{TiO})}} + 0.5p(\text{LaO})\sqrt{\frac{M(\text{O})}{M(\text{LaO})}}. \quad (3)$$

The vaporization rates of the samples were determined using the partial pressures of the vapor species by Eq. (4), which is a transformed form of Eq. (1):

$$\frac{q_i}{ts} = p_i L \sqrt{\frac{M_i}{2\pi RT}}, \quad (4)$$

where q_i/ts is the mass of the i vapor species that vaporized from the unit sample surface s during unit time t .

It should be highlighted that the effusion cell, from which samples are vaporized in the KEMS studies, cannot be opened because the lids of the effusion cells are closely connected with the cell crucible. So, the samples under examination could not be extracted for the subsequent analysis after the high-temperature experiments. To purify the effusion cell, the samples were vaporized completely at high temperatures. This technique has an advantage because it allows determination of the concentration dependences of the thermodynamic properties in the system under study. If a sample is vaporized completely and ion current intensities in mass spectra of vapor over it are measured simultaneously, then changes in the sample condensed phase composition due to the component vaporization can be evaluated by the complete isothermal vaporization method. This enables thermodynamic properties to be obtained for all the condensed phase compositions observed in the course of the sample vaporization using the standard KEMS technique, for instance, determination of partial pressures of vapor species and vaporization rates of all the observed condensed phase compositions by Eqs. (2)-(4).

3. Results and discussion

3.1. Sample N 1: 90 mole % TiO₂

In the mass spectrum over sample N 1, the ion peaks of TiO⁺ and TiO₂⁺ with the intensity ratio 1:0.9 were recorded starting from the temperature of 2000 K. No peaks referring to lanthanum were detected at this temperature. Transition of lanthanum oxide to the vapor phase started at the temperature about 2270 K when LaO⁺ ions appeared in mass spectra. During isothermal vaporization at 2290 K, the intensities of the TiO₂⁺ and TiO⁺ ion currents gradually decreased while the LaO⁺ ion current increased. The ratio of the TiO⁺ and TiO₂⁺ ion currents first increased steadily from nearly 0.5 to 1.6, and then for a long while remained constant. As the temperature was raised up to 2590 K, all ion currents increased and then dropped to the level of background indicating complete vaporization of the sample.

For the mass spectra interpretation, the appearance energies of the ions were measured. The obtained values of 9.6 (TiO₂⁺), 6.7 (TiO⁺), and 5.0 (LaO⁺) eV were equal within the accuracy of the measurements (± 0.3 eV) to the energies of ionization of the corresponding molecules

[35] proving that the main vapor species over the sample under study were TiO₂, TiO, LaO, and oxygen.

Thus, the vaporization of this sample in the La₂O₃-TiO₂ system can be described by the following reactions:



The results of calculations by Eqs. (2) and (3) are listed in Table 2. The dynamics of the sample mass losses due to the component vaporization at high temperatures calculated by Eq. (4) is presented in Table S1 in Supporting Information.

The partial pressures of the vapor species over sample N 1 as a function of vaporization time and temperature are shown in Fig. S3 (Supporting information).

On the basis of the obtained data, Table 2, the mass loss of the sample with time was calculated allowing for the calculation of the dependence of the partial pressures on the composition of condensed phase. The resulting curves are shown in Fig. 1. It follows from this figure that the ratio of TiO to TiO₂ partial pressures increased in the first part of the experiment at the temperature 2290 K from 0.21 to 0.67 and then remained constant in the range 0.74 ± 0.07 practically until the temperature increase to 2590 K.

From the experimental data on the temperature dependences of the TiO₂ and TiO partial pressures in the vapor over sample N 1, the following equations, Eqs. (8) and (9), could be derived in the temperature range 2019–2221 K:

$$\log p(\text{TiO}_2, \text{Pa}) = -\frac{18506 \pm 1689}{T} + (8.22 \pm 0.78), \quad (8)$$

Table 2

Partial pressures of the vapor species over the La₂O₃-TiO₂ system vaporizing from the initial composition La₂O₃:TiO₂ = 10:90, mole %, as a function of the vaporization time, temperature, and composition of the condensed phase. The standard uncertainty of the partial pressures of the TiO₂, TiO, and LaO vapor species over the sample under study is 15 %.

Vaporization time, min	T, K	x _i , mole fraction		p _i , Pa			
		TiO ₂	La ₂ O ₃	TiO ₂	TiO	LaO	O
2	2019	0.900	0.100	0.23	0.08	–	0.04
6	2091	0.900	0.100	0.50	0.20	–	0.10
10	2124	0.899	0.101	0.89	0.12	0.01	0.06
13	2207	0.899	0.101	1.49	0.34	0.02	0.17
17	2221	0.898	0.102	1.31	0.24	0.02	0.12
20	2289	0.897	0.103	3.29	0.68	0.04	0.35
25	2289	0.895	0.105	3.00	0.81	0.04	0.41
30	2284	0.893	0.107	2.80	1.09	0.04	0.55
35	2284	0.890	0.110	2.61	1.16	0.04	0.58
40	2284	0.887	0.113	2.61	1.20	0.05	0.61
50	2290	0.882	0.118	2.13	1.23	0.06	0.62
60	2289	0.877	0.123	1.93	1.30	0.09	0.66
70	2288	0.871	0.129	2.03	1.28	0.09	0.65
90	2287	0.859	0.141	1.74	1.11	0.11	0.57
100	2285	0.852	0.148	1.64	1.29	0.11	0.66
120	2284	0.837	0.163	1.45	1.06	0.13	0.55
135	2287	0.825	0.175	1.45	1.06	0.13	0.55
150	2290	0.811	0.189	1.16	0.84	0.13	0.44
165	2288	0.796	0.204	1.16	0.92	0.10	0.48
180	2285	0.779	0.221	0.96	0.73	0.10	0.38
195	2286	0.761	0.239	0.87	0.70	0.09	0.36
210	2288	0.741	0.259	0.77	0.63	0.10	0.33
240	2296	0.694	0.306	0.68	0.60	0.13	0.32
240	2586	0.694	0.306	7.22	6.87	3.50	3.99
245	2586	0.634	0.366	4.59	5.75	4.20	3.55
250	2580	0.593	0.407	2.84	3.43	5.12	2.53
255	2582	0.674	0.326	–	0.83	0.62	0.51
260	2585	0.899	0.101	–	0.14	0.06	0.08

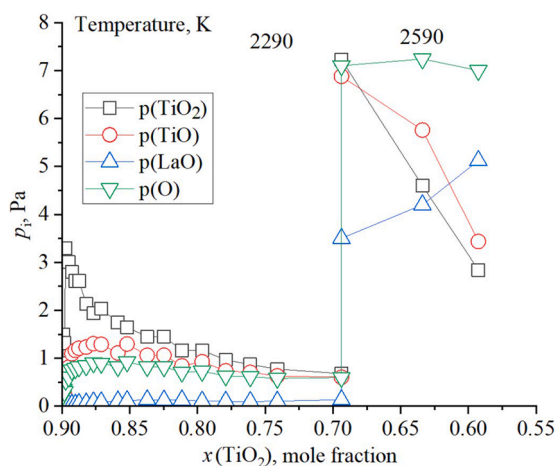


Fig. 1. Concentration dependence of the partial pressures of vapor species over sample N 1, containing initially 90 mole % TiO_2 , at 2290 K and 2590 K.

$$\log p(\text{TiO}, \text{Pa}) = -\frac{15255 \pm 2172}{T} + (6.40 \pm 1.01), \quad (9)$$

which are presented graphically in Fig. S4 (Supporting information). It should be mentioned that Eqs. (8) and (9) are ascribed to the initial composition of the sample. The condensed phase composition could be assumed as not changing in the experimental runs. To ensure this, a much larger mass of the sample was loaded into the effusion cell compared to the complete vaporization experiments to guarantee the correctness of the obtained values. It is known that changes in the condensed phase composition manifest itself by the changes in the TiO_2^+ and TiO^+ ion currents at a certain fixed temperature T . At the instant when the ion current intensities (measured at the temperature T) started to decrease, the experiment was stopped, and, thus, only the data obtained at nearly constant composition were used for derivation of Eqs. (8) and (9). Hence, the equations are valid for the composition of 10 mole % La_2O_3 and 90 mole % TiO_2 , i.e. for the initial composition of the sample.

3.2. Sample N 2: 50 mole % TiO_2

The peaks of TiO^+ and TiO_2^+ ion currents appeared in the mass spectrum of the vapor over sample N 2 at the temperature around 2400 K. Simultaneously a more intensive peak of the LaO^+ ion was recorded. The measured appearance energies of the ions indicated that the molecular species in the vapor over sample N 2 were the same as over sample N 1 (TiO_2 , TiO , LaO , and O). In the course of isothermal vaporization of the sample at the temperature 2475 K, the LaO^+ ion current gradually decreased while the TiO^+ and TiO_2^+ currents increased. As it was mentioned in Section 2.2, samples NN 1 and 2 were vaporized completely at high temperatures to remove the sample residues from the Knudsen cell, and mass spectra of vapor over them were simultaneously measured. This can be seen in Figs. S3 and S5 (Supporting information) as the gradual decrease in the partial pressures of the vapor species over samples NN 1 and 2 with vaporization time in the final parts of the KEMS experiments.

The partial pressures of the vapor species over sample N 2 were determined using Eq. (2). Dependence of the partial pressures of the vapor species over sample N 2 on the vaporization time is shown in Fig. S5 (Supporting information). Using these curves and the complete isothermal vaporization method similarly to sample N 1, the dependence of the partial pressures on the composition of the condensed phase was derived, Fig. 2.

The data on the partial pressures of vapor species over sample N 2 depending on the vaporization time, composition of condensed phase,

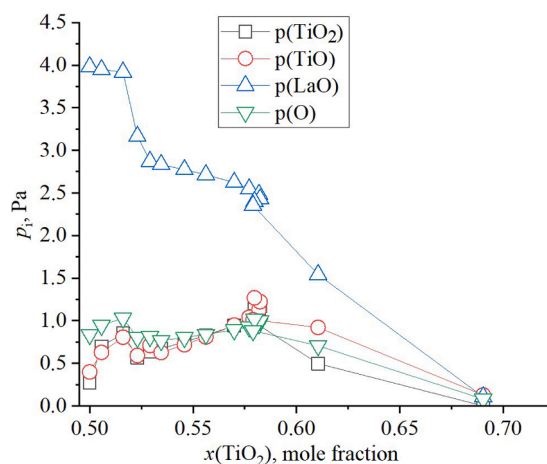


Fig. 2. Partial pressures of vapor species over sample N 2, containing initially 50 mole % TiO_2 , as a function of condensed phase composition at the temperature 2475 K.

and temperature are listed in Table 3. The dynamics of the sample mass losses due to the component vaporization at high temperatures calculated by Eq. (4) is presented in Table S2 in Supporting Information.

The temperature dependence of the vapor species partial pressures was not obtained since the partial pressures of TiO , TiO_2 , and LaO could not be measured in a sufficiently wide temperature range due to the big difference in the volatilities of titanium and lanthanum oxides. When TiO^+ and TiO_2^+ appeared in the mass spectrum the intensity of LaO^+ started to decrease rapidly indicating a considerable change in the composition of condensed phase.

The difference in the most volatile components in samples NN 1 and 2 should be especially mentioned. As follows from Table 2, titanium oxide vaporized predominantly from sample N 1, containing initially 90 mole % TiO_2 . The condensed phase in course of the vaporization was enriched with La_2O_3 . In contrast, sample N 2, containing initially 50 mole % TiO_2 , was characterized by predominant vaporization of lanthanum oxide while the condensed phase was enriched with TiO_2 . This evidences that an azeotrope may exist in the concentration range 50–90 mole % TiO_2 between the samples studied. According to our

Table 3

Partial pressures of vapor species over the La_2O_3 - TiO_2 system with the initial composition La_2O_3 : $\text{TiO}_2 = 50:50$, mole %, as a function of vaporization time, temperature, and composition of the condensed phase. The standard uncertainty of the partial pressures of the TiO_2 , TiO , and LaO vapor species over the sample under study is 15 %.

Vaporization time, min	T, K	x_i , mole fraction		p_i , Pa			
		TiO_2	La_2O_3	TiO_2	TiO	LaO	O
0	2416	0.500	0.500	0.27	0.40	3.98	0.84
3	2440	0.506	0.494	0.70	0.63	3.95	0.94
10	2469	0.51	0.484	0.84	0.80	3.91	0.94
15	2469	0.52	0.477	0.56	0.59	3.16	1.03
20	2475	0.529	0.471	0.63	0.70	2.87	0.80
25	2469	0.535	0.465	0.67	0.62	2.83	0.81
35	2469	0.546	0.454	0.75	0.71	2.77	0.76
45	2470	0.556	0.444	0.82	0.80	2.71	0.80
60	2470	0.570	0.430	0.94	0.94	2.62	0.83
70	2469	0.577	0.423	1.01	1.03	2.54	0.89
80	2467	0.582	0.418	1.08	1.12	2.48	0.92
90	2472	0.582	0.418	1.16	1.22	2.42	0.96
95	2472	0.580	0.420	1.20	1.26	2.39	1.00
105	2472	0.579	0.421	0.99	1.01	2.35	1.01
125	2476	0.610	0.390	0.49	0.92	1.54	0.88
135	2478	0.690	0.310	–	0.12	0.10	0.70
150	2478	–	–	–	–	–	–

evaluation based on the complete isothermal vaporization experiments, which allowed calculation of the changes in the condensed phase chemical compositions of the samples due to the component selective vaporization, the azeotrope composition should contain 60 to 70 mole % TiO_2 . However, there is a need for separate experiments with the samples in the concentration range mentioned to show that their condensed phase chemical composition remains unchanged and no selective vaporization of the components takes place at temperatures as high as 2475 K. These experiments would allow identification of the azeotropic composition in the La_2O_3 - TiO_2 system more precisely and can become the base for continuation of the present investigation in subsequent studies.

3.3. Thermodynamic properties of the La_2O_3 - TiO_2 system

Differential mass spectrometry method used in the present study permits determination of component activities without calculating the partial pressures, Eq. (1), which may introduce additional uncertainties to the obtained values. When reference effusion cell is loaded with individual titanium dioxide, then the TiO_2 activity is determined using Eq. (10)

$$a(\text{TiO}_2) = \frac{p(\text{TiO}_2)}{p^*(\text{TiO}_2)} = \frac{I(\text{TiO}_2^+)}{I^*(\text{TiO}_2^+)}, \quad (10)$$

where subscript “ \circ ” refers to the activity standard (pure TiO_2). The partial pressures in Eq. (10) are substituted for the corresponding ion currents according to Eq. (11)

$$p_i = kI_i T, \quad (11)$$

where k is the sensitivity constant of the device. Concentration dependence of the TiO_2 activity determined by Eq. (10) is represented in Table 4 and in Fig. 3.

The range of compositions shown in Fig. 3 is divided into two sections. The right hand part summarizes the results of isothermal vaporization of sample N 1 (90 mole % TiO_2) at the temperature 2290 K and the left hand part refers to sample N 2 (50 mole % TiO_2) vaporized at the temperature 2475 K. It should be mentioned that it was impossible to measure the titanium dioxide activity from the isothermal vaporization of sample N 1 for the whole range of compositions shown in Fig. 3.

Table 4

Concentration dependence of the component activities, Gibbs energy of formation from the oxides (ΔG), and excess Gibbs energy (ΔG^E) in La_2O_3 - TiO_2 melt.

x_i , mole fractions		T , K	a_i		$-\Delta G$ (± 6 kJ/mole), kJ/mole	$-\Delta G^E$ (± 6 kJ/mole), kJ/mole
TiO_2	La_2O_3		TiO_2	La_2O_3		
0.900	0.100	2290	0.84	9×10^{-5}	23	17
0.875	0.125		0.72	3×10^{-4}	28	21
0.850	0.150		0.63	7×10^{-4}	33	25
0.825	0.175		0.54	1.6×10^{-3}	37	28
0.800	0.200		0.47	2.8×10^{-3}	41	32
0.775	0.225		0.41	4.7×10^{-3}	45	35
0.750	0.250		0.35	7.8×10^{-3}	49	38
0.725	0.275		0.31	0.011	52	41
0.700	0.300		0.27	0.016	55	43
0.600	0.400	2475	0.165	0.039	61	49
0.575	0.425		0.145	0.046	62	49
0.550	0.450		0.12	0.059	62	49
0.525	0.475		0.098	0.075	61	48
0.500	0.500		0.071	0.11	61	47

When, as a result of mass loss, the content of TiO_2 reached 70 mole %, the composition of condensed phase stabilized and did not change during further vaporization. The curves in Fig. 3 indicate also that TiO_2 activity does not depend on the temperature significantly.

Fig. 4 represents the phase diagram of the La_2O_3 - TiO_2 system given in Refs. [36–38]. Vaporization of both samples was carried out at the temperatures corresponding to the field of homogeneous melts on the phase diagram. Hence, the activity of the second component can be calculated using Gibbs-Duhem integration, Eq. (12):

$$\ln \frac{a(\text{La}_2\text{O}_3)}{x(\text{La}_2\text{O}_3)} = - \int_{\ln \frac{a^0(\text{TiO}_2)}{x^0(\text{TiO}_2)}}^{\ln \frac{a(\text{TiO}_2)}{x(\text{TiO}_2)}} \frac{x(\text{TiO}_2)}{x(\text{La}_2\text{O}_3)} d \ln \frac{a(\text{TiO}_2)}{x(\text{TiO}_2)}. \quad (12)$$

However, strong deviation of TiO_2 activity concentration dependence from the ideal behavior did not allow its correct extrapolation to $x(\text{TiO}_2) = 0$, which must be carried out according to Eq. (12). To avert this difficulty, the Redlich-Kister polynomial approximation [39] and modeling within the GLTAS approach [40] were performed (see next section). The results obtained by the Redlich-Kister polynomial are presented in Supporting information in Figs. S6 and S7 and Table S3. The GLTAS results are presented in Table 4 and in Figs. 3 and 5. The ΔG and ΔG^E errors shown in Table 4 were calculated based on the deviations of the TiO_2 activities and activity coefficients obtained experimentally and optimized using the GLTAS approach as presented in Fig. 3 for the TiO_2 activities.

3.4. Modeling

The generalized lattice theory of associated solutions (GLTAS) [40] is quite suitable for analysis and extrapolation of the experimental data obtained by Knudsen effusion mass spectrometry and has been repeatedly used for optimization of various oxide systems [41,42]. A brief account of the theory may be found in the Supporting information.

In the present study the following model was chosen. The coordination number of the model lattice equals 4. TiO_2 and La_2O_3 are the structural units occupying 1 and 2 sites of the lattice, respectively, according to the molar volumes of the oxides, and have 4 and 6 contact points. The energies of interaction of contacts metal-metal and oxygen-oxygen are considered zero.

Analysis of the data on the energy parameters obtained earlier in several binary and ternary systems indicates that, for the same oxides, they do not vary greatly, within the accuracy of calculations, in groups of ternary and multicomponent systems containing these oxides. Since the experimental data were available only for one component, the energy parameters could be interpolated only with great uncertainties, thereby making the results of the calculations rather indeterminate. This difficulty could be partly eliminated by making use of transferability of the energy parameters, i.e., the values for La-O[La] and Ti-O[Ti] bonds taken from our earlier studies [43,44]. As a result, the optimized concentration dependences of the TiO_2 and La_2O_3 activities and excess Gibbs energies were obtained, Figs. 3 and 5. Taking as a reference the calculated values for $a(\text{La}_2\text{O}_3)$, curve 2 in Fig. 3, the Gibbs-Duhem integration of $a(\text{TiO}_2)$ was normalized, the calculated values of the La_2O_3 activities are shown in the figure.

Additionally, GLTAS approach allows comparison of the obtained thermodynamic functions with the relative number of bonds of different type in the lattice modeling the melt structure, Fig. 6. Maximum of the curve 3 for mixed bonds in the figure is shifted towards greater concentrations of TiO_2 . The same behavior demonstrates ΔG^E in Fig. 5. This is in full agreement with the phase diagram shown in Fig. 4 and indicates that the strongest interaction of components in the melts corresponds to the compound $\text{La}_2\text{O}_3 \bullet 2\text{TiO}_2$, existing at lower temperatures.

The strong negative deviations observed in the La_2O_3 - TiO_2 system are unfavorable for determination of thermodynamic properties by

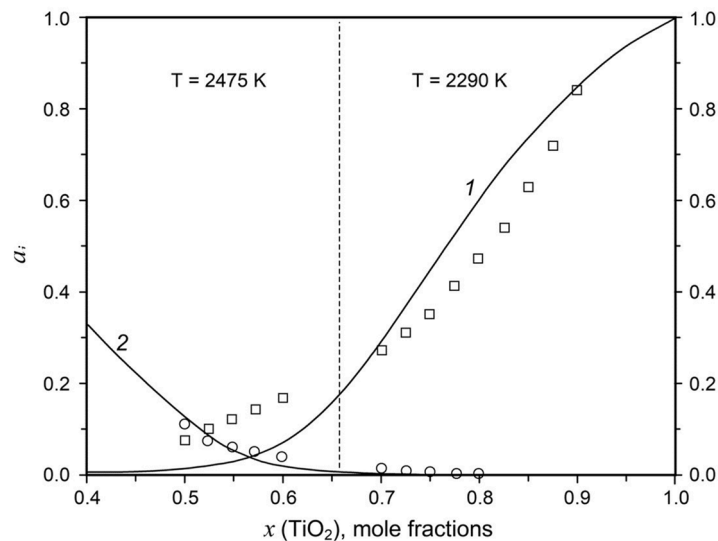


Fig. 3. The TiO_2 and La_2O_3 activities in the La_2O_3 - TiO_2 system as a function of the condensed phase composition. 1 is TiO_2 , 2 is La_2O_3 , \square is the experimental TiO_2 activity value, $^\circ$ is the La_2O_3 activity obtained by the Gibbs-Duhem equation.

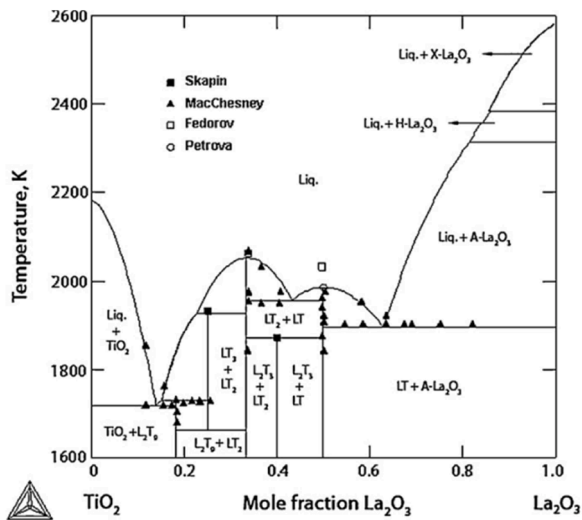


Fig. 4. Phase diagram of the La_2O_3 - TiO_2 system according to Refs. [36–38].

KEMS in two respects. First, the lower values of ion currents resulting from the strong negative deviations lead to the lower measurement accuracy and, hence, to greater uncertainties of the obtained values and reduced concentration range available for the KEMS study due to the sensitivity limitations of the mass spectrometer. Second, the strong negative deviations reduce the accuracy of determination of component activity by the differential mass spectrometric method since the values of partial pressures of vapor species over a sample p_i and a standard p_i° , which are to be measured, may differ by orders of magnitude. Two limitations define the available range of the vaporization temperatures in KEMS: at low temperatures, though p_i° may still remain within the range of the validity of the Knudsen method, p_i approaches the threshold of the method sensitivity and becomes too low to be measured. At too high temperatures, when p_i can be measured with sufficient precision, p_i° becomes greater than 13 Pa, which is considered as the maximum vapor pressure that can be reliably determined by the Knudsen effusion method. So, it is necessary to find the temperature at which p_i is slightly above the sensitivity threshold while p_i° is still within the range of the validity of the KEMS method, which is certain to increase the uncertainty of the values obtained. Third, the resulting steep concentration

dependences of the component activities can only roughly be interpolated within the GLTAS approach. This factor explains certain disagreement between the TiO_2 activities obtained experimentally and calculated by the GLTAS optimization, Fig. 3. Hence, the given thermodynamic description should be considered as semi-quantitative. The main finding of the present study is the achievement of the stage of congruent vaporization in samples NN 1 and 2, implying the existence of a certain azeotropic composition in the range of melt concentrations from 60 to 70 mole % TiO_2 .

4. Conclusions

First, thermodynamic description of La_2O_3 - TiO_2 melts at the temperatures 2290 K and 2475 K was obtained using the Knudsen effusion mass spectrometric method. Vaporization dynamics of these melts at the temperatures mentioned illustrated the possibility of the azeotrope formation in the La_2O_3 - TiO_2 system. Modeling of the thermodynamic data with the correlation of the structure of the condensed phase of the La_2O_3 - TiO_2 melts was carried out using the generalized lattice theory of associated solutions. The experimental data found may be used in the further modeling of the phase equilibria using the CALPHAD approach.

Financial support

The study was supported by the Russian Science Foundation [grant number 23-13-00254, <https://rscf.ru/en/project/23-13-00254/>].

CRediT authorship contribution statement

Valentina L. Stolyarova: Writing – review & editing, Supervision, Project administration, Funding acquisition. **Andrey L. Shilov:** Writing – original draft, Visualization, Formal analysis, Data curation. **Viktor A. Vorozhtcov:** Writing – review & editing, Visualization, Formal analysis. **Sergey I. Lopatin:** Writing – original draft, Visualization, Investigation, Data curation. **Anna V. Fedorova:** Resources, Investigation.

Declaration of competing interest

The authors declare the following financial interests/personal relationships which may be considered as potential competing interests: Valentina L. Stolyarova, Andrey L. Shilov, Viktor A. Vorozhtcov, Sergey I. Lopatin, Anna V. Fedorova report financial support was provided by

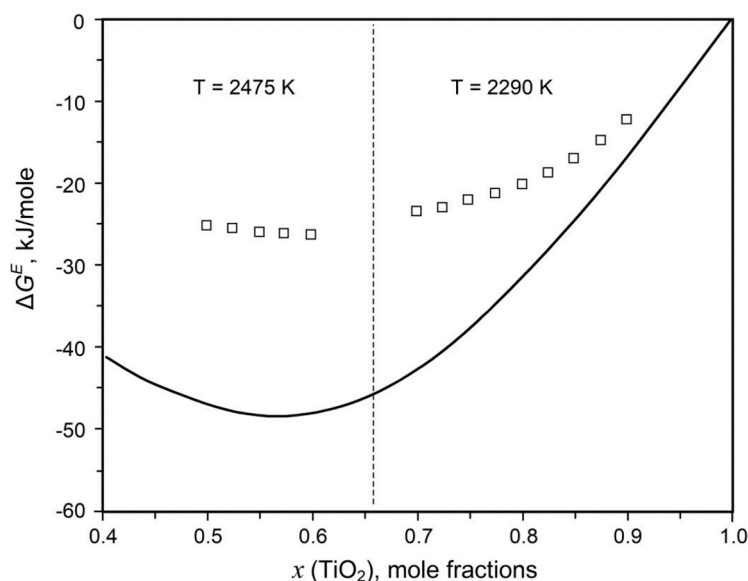


Fig. 5. Excess Gibbs energy (ΔG^E) in $\text{La}_2\text{O}_3\text{-TiO}_2$ melt as a function of the composition calculated from the component activities optimized by GLTAS modeling. \square is the values obtained by the Gibbs-Duhem equation.

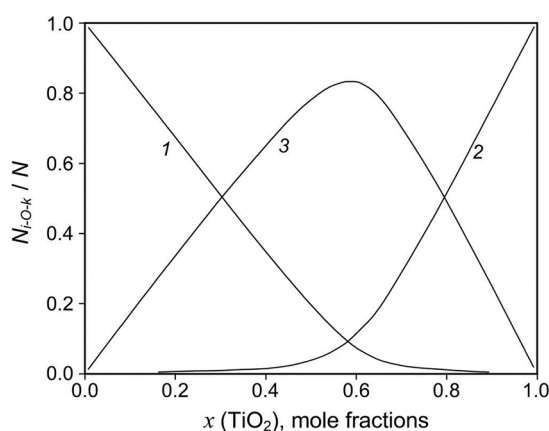


Fig. 6. The relative number of bonds in the lattice model of the $\text{La}_2\text{O}_3\text{-TiO}_2$ system when the second coordination sphere was taken into consideration. 1 is La-O[La], 2 is Ti-O[Ti], 3 is La-O[Ti].

the Russian Science Foundation. If there are other authors, they declare that they have no known competing financial interests or personal relationships that could have appeared to influence the work reported in this paper.

Acknowledgements

The authors are grateful to the Cryogenic department of the Research Park of Saint Petersburg State University for the uninterrupted supply of liquid nitrogen for the mass spectrometer. The X-ray phase analysis and X-ray fluorescence analysis of the samples were carried out using the equipment of the Research Park of Saint Petersburg State University in the Research Centre for X-ray Diffraction Studies and in Chemical Analysis and Materials Research Centre, respectively.

Supplementary materials

Supplementary material associated with this article can be found, in the online version, at [doi:10.1016/j.ctta.2025.100164](https://doi.org/10.1016/j.ctta.2025.100164).

Data availability

Data will be made available on request.

References

- [1] C. Oses, C. Toher, S. Curtarolo, High-entropy ceramics, *Nat. Rev. Mater.* 5 (2020) 295–309, <https://doi.org/10.1038/s41578-019-0170-8>.
- [2] M. Anandkumar, E. Trofimov, Synthesis, properties, and applications of high-entropy oxide ceramics: current progress and future perspectives, *J. Alloys Compd.* 960 (2023) 170690, <https://doi.org/10.1016/j.jallcom.2023.170690>.
- [3] Z. Wen, Z. Tang, H. Meng, Y. Chu, A promising new class of high-entropy ceramics: high-entropy oxycarbides with good oxidation resistance, *Corros. Sci.* 207 (2022) 110574, <https://doi.org/10.1016/j.corsci.2022.110574>.
- [4] W. Song, Y. Lu, C. Wang, J. Xu, X. Liu, B. Ma, Y. Wang, B. Wu, Atomic arrangement and mechanical properties of high-entropy nonoxide ceramics simulated via location preference-based disordered random structure, *J. Alloys Compd.* (2024) 175455, <https://doi.org/10.1016/j.jallcom.2024.175455>.
- [5] Z. Li, J. Li, H. Zhao, M. Zhang, P. Li, L. Dong, L. Wu, H. Ji, X. Qi, Influence of atmosphere-induction and synergistic effect on the dielectric property of rutile-type ($\text{Ge}_0.2\text{Mn}_0.2\text{Ti}_0.2\text{Sn}_0.2\text{Mo}_0.2$)O₂ high-entropy oxides, *J. Alloys Compd.* 1002 (2024) 175246, <https://doi.org/10.1016/j.jallcom.2024.175246>.
- [6] D. Jia, T. Chigan, X. Li, H. Li, P. Yang, Photocatalytic degradation performance for high-entropy oxide ($\text{La}_0.2\text{Ce}_0.2\text{Gd}_0.2\text{Zr}_0.2\text{Fe}_0.2$)O₂ enriched with defects, *J. Alloys Compd.* 982 (2024) 173808, <https://doi.org/10.1016/j.jallcom.2024.173808>.
- [7] Ö. Güler, D. Yilmaz, M.S. Kanca, K. Edalati, Y. Taşgun, Radiation shielding properties of composites of TiZrNbHfTa refractory high entropy alloy reinforced with TiZrNbHfTaOx high-entropy oxide, *J. Alloys Compd.* 995 (2024) 174815, <https://doi.org/10.1016/j.jallcom.2024.174815>.
- [8] Y. Wang, Processing and properties of high entropy carbides, *Adv. Appl. Ceram.* 121 (2022) 57–78, <https://doi.org/10.1080/17436753.2021.2014277>.
- [9] H. Chen, H. Xiang, F.Z. Dai, J. Liu, Y. Lei, J. Zhang, Y. Zhou, High porosity and low thermal conductivity high entropy ($\text{Zr}_0.2\text{Hf}_0.2\text{Ti}_0.2\text{Nb}_0.2\text{Ta}_0.2$)C, *J. Mater. Sci. Technol.* 35 (2019) 1700–1705, <https://doi.org/10.1016/j.jmst.2019.04.006>.
- [10] Y. Dong, K. Ren, Y. Lu, Q. Wang, J. Liu, Y. Wang, High-entropy environmental barrier coating for the ceramic matrix composites, *J. Eur. Ceram. Soc.* 39 (2019) 2574–2579, <https://doi.org/10.1016/j.jeurceramsoc.2019.02.022>.
- [11] A. Klimkowicz, K. Świerczek, A. Takasaki, B. Dabrowski, Oxygen storage capability in Co- and Fe-containing perovskite-type oxides, *Solid State Ion* 257 (2014) 23–28, <https://doi.org/10.1016/j.ssi.2014.01.018>.
- [12] J. Adánez, L.F. De Diego, F. García-Labiano, P. Gayán, A. Abad, J.M. Palacios, Selection of oxygen carriers for chemical-looping combustion, *Energy Fuels* 18 (2004) 371–377, <https://doi.org/10.1021/ef0301452>.
- [13] J.W. Lekse, S. Natesakhawat, D. Alfonso, C. Matranga, An experimental and computational investigation of the oxygen storage properties of $\text{BaLnFe}_2\text{O}_5+\delta$ and $\text{BaLnCo}_2\text{O}_5+\delta$ (Ln = La, Y) perovskites, *J. Mater. Chem. A* 2 (2014) 2397–2404, <https://doi.org/10.1039/c3ta13257a>.
- [14] L. Nalbandian, A. Evdou, V. Zaspalis, $\text{La}_1\text{-xSr}_x\text{MyFe}_1\text{-yO}_3\text{-}\delta$ perovskites as oxygen-carrier materials for chemical-looping reforming, *Int. J. Hydrog. Energy* 36 (2011) 6657–6670, <https://doi.org/10.1016/j.ijhydene.2011.02.146>.

- [15] A. Amiri, R. Shahbazian-Yassar, Recent progress of high-entropy materials for energy storage and conversion, *J. Mater. Chem. A* 9 (2021) 782–823, <https://doi.org/10.1039/d0ta09578h>.
- [16] J. Yan, D. Wang, X. Zhang, J. Li, Q. Du, X. Liu, J. Zhang, X. Qi, A high-entropy perovskite titanate lithium-ion battery anode, *J. Mater. Sci.* 55 (2020) 6942–6951, <https://doi.org/10.1007/s10853-020-04482-0>.
- [17] H.-L. Liu, Z.-Y. Man, J.-X. Liu, X.-G. Wang, G.-J. Zhang, Solid solution and densification behavior of zirconium oxycarbide (ZrCxOy) ceramics via doping ZrO₂ and Zr in ZrC, *J. Alloys Compd.* 729 (2017) 492–497, <https://doi.org/10.1016/j.jallcom.2017.09.183>.
- [18] V.I. Almjashv, V.L. Stolyarova, E.V. Krushinov, A.A. Sulatsky, E.B. Shuvaeva, A. V. Timchuk, E.V. Shevchenko, S.Yu. Kotova, S.A. Vitol, E.K. Kalyago, V.R. Bulygin, E.M. Belyaeva, I.E. Arlashkin, S.N. Perevislov, D.P. Danilovich, V.B. Khabensky, Investigation of high temperature interaction between materials containing MAX phases and chemical prototype of VVER core melt, *Nucl. Propuls. React. Plants Life Cycle Manag. Technol.* 31 (2023) 60–75, https://doi.org/10.52069/2414-5726_2023_1_31_60.
- [19] J. Drowart, C. Chatillon, J. Hastie, D. Bonnell, High-temperature mass spectrometry: instrumental techniques, ionization cross-sections, pressure measurements, and thermodynamic data (IUPAC Technical Report), *Pure Appl. Chem.* 77 (2005) 683–737, <https://doi.org/10.1351/pac200577040683>.
- [20] N.S. Jacobson, J.-Y. Colle, V. Stolyarova, T. Markus, I. Nuta, Knudsen effusion mass spectrometry: current and future approaches, *Rapid Commun. Mass Spectrom.* 38 (2024) e9744, <https://doi.org/10.1002/rcm.9744>.
- [21] S.I. Lopatin, S.M. Shugurov, Z.G. Tyurnina, N.G. Tyurnina, Ti₃O₅ and V₂O₃ vaporization, *Glass Phys. Chem.* 47 (2021) 38–41, <https://doi.org/10.1134/S1087659621010077>.
- [22] S.I. Lopatin, Vaporization and thermodynamic properties of the NbO₂-TiO₂ system, *Glass Phys. Chem.* 48 (2022) 117–122, <https://doi.org/10.1134/S1087659622020055>.
- [23] E.N. Kablov, V.L. Stolyarova, V.A. Vorozhtcov, S.I. Lopatin, F.N. Karachevtsev, Thermodynamics and vaporization of ceramics based on the Y₂O₃-ZrO₂ system studied by KEMS, *J. Alloys Compd.* 794 (2019) 606–614, <https://doi.org/10.1016/j.jallcom.2019.04.208>.
- [24] E.N. Kablov, A.L. Shilov, V.L. Stolyarova, F.N. Karachevtsev, S.I. Lopatin, S. M. Shugurov, V.A. Vorozhtcov, Thermodynamics and vaporization of ceramics based on the Gd₂O₃-ZrO₂ and Gd₂O₃-HfO₂ systems studied by KEMS, *J. Alloys Compd.* 908 (2022) 164575, <https://doi.org/10.1016/J.JALLCOM.2022.164575>.
- [25] N.G. Tyurnina, S.I. Lopatin, E.A. Balabanova, S.M. Shugurov, Z.G. Tyurnina, I. G. Polyakova, Thermodynamic properties of the BaO-Al₂O₃ system, *J. Alloys Compd.* 969 (2023) 172266, <https://doi.org/10.1016/j.jallcom.2023.172266>.
- [26] L.L. Ames, P.N. Walsh, D. White, Rare earths. IV. Dissociation energies of the gaseous monoxides of the rare earths, *J. Phys. Chem.* 71 (1967) 2707–2718, <https://doi.org/10.1021/j100867a049>.
- [27] R.J. Ackermann, E.G. Rauh, A high temperature study of the stoichiometry, phase behavior, vaporization characteristics, and thermodynamic properties of the lanthanum+oxygen system, *J. Chem. Thermodyn.* 3 (1971) 445–460, [https://doi.org/10.1016/S0021-9614\(71\)80027-7](https://doi.org/10.1016/S0021-9614(71)80027-7).
- [28] P.W. Gilles, K.D. Carlson, H.F. Franzen, P.G. Wahlbeck, High-temperature vaporization and thermodynamics of the titanium oxides. I. Vaporization characteristics of the crystalline phases, *J. Chem. Phys.* 46 (1967) 2461–2465, <https://doi.org/10.1063/1.1841070>.
- [29] P.J. Hampson, P.W. Gilles, High-temperature vaporization and thermodynamics of the titanium oxides. VII. Mass spectrometry and dissociation energies of TiO(g) and TiO₂(g), *J. Chem. Phys.* 55 (1971) 3708–3711, <https://doi.org/10.1063/1.1676654>.
- [30] L.V. Gurvich, I.V. Veitz, V.A. Medvedev, G.A. Khachkuruzov, V.S. Jungman, G. A. Bergman, V.F. Baybuz, *Thermodynamic Properties of Individual Substances*, Nauka, Moscow, 1979.
- [31] R.C. Paule, J. Mandel, Analysis of interlaboratory measurements on the vapor pressure of cadmium and silver, *Pure Appl. Chem.* 31 (1972) 395–432, <https://doi.org/10.1351/pac197231030395>.
- [32] J.B. Mann, Ionization cross sections of the elements calculated from mean-square radii of inner orbitals, *J. Chem. Phys.* 46 (1967) 1646–1651, <https://doi.org/10.1063/1.1840917>.
- [33] P.L. Zeifert, Measurement of vapor pressure of refractories, in: I.E. Kempbell (Ed.), *High Temp. Technol.*, John Wiley, New York, 1956, pp. 485–496.
- [34] E.N. Kablov, V.L. Stolyarova, S.I. Lopatin, V.A. Vorozhtcov, F.N. Karachevtsev, Y. I. Folomeikin, Mass spectrometric study of thermodynamic properties in the Gd₂O₃-Y₂O₃ system at high temperatures, *Rapid Commun. Mass Spectrom.* 31 (2017) 538–546, <https://doi.org/10.1002/rcm.7809>.
- [35] S.G. Lias, J.E. Bartmess, J.F. Liebman, J.L. Holmes, R.D. Levin, W.G. Mallard, *Gas-phase ion and neutral thermochemistry*, *J. Phys. Chem. Ref. Data* 17 (1988) 861.
- [36] J.B. McChesney, H.A. Sauer, The system La₂O₃-TiO₂; phase equilibria and electrical properties, *J. Am. Ceram. Soc.* 45 (1962) 416–422, <https://doi.org/10.1111/j.1151-2916.1962.tb11185.x>.
- [37] M.A. Petrova, A.S. Novikova, R.G. Grebenschikov, Phase Relations in the pseudobinary systems La₂TiO₅-Lu₂TiO₅ and Gd₂TiO₅-Tb₂TiO₅, *Inorg. Mater.* 39 (2003) 509–513, <https://doi.org/10.1023/A:1023628812895>.
- [38] S.D. Škapin, D. Kolar, D. Suvorov, Phase stability and equilibria in the La₂O₃-TiO₂ system, *J. Eur. Ceram. Soc.* 20 (2000) 1179–1185, [https://doi.org/10.1016/S0955-2219\(99\)00270-8](https://doi.org/10.1016/S0955-2219(99)00270-8).
- [39] O. Redlich, A.T. Kister, Algebraic representation of thermodynamic properties and the classification of solutions, *Ind. Eng. Chem.* 40 (1948) 345–348, <https://doi.org/10.1021/ie50458a036>.
- [40] J.A. Barker, Cooperative orientation effects in solutions, *J. Chem. Phys.* 20 (1952) 1526–1532, <https://doi.org/10.1063/1.1700209>.
- [41] A.L. Shilov, V.L. Stolyarova, S.I. Lopatin, V.A. Vorozhtcov, Thermodynamic properties of the Gd₂O₃-Y₂O₃-HfO₂ system studied by high temperature Knudsen effusion mass spectrometry and optimized using the Barker lattice theory, *J. Alloys Compd.* 791 (2019) 1207–1212, <https://doi.org/10.1016/J.JALLCOM.2019.03.182>.
- [42] A.L. Shilov, V.L. Stolyarova, V.A. Vorozhtcov, S.I. Lopatin, Thermodynamic description of the Gd₂O₃-Y₂O₃-HfO₂ and La₂O₃-Y₂O₃-HfO₂ systems at high temperatures, *Calphad* 65 (2019) 165–170, <https://doi.org/10.1016/J.CALPHAD.2019.03.001>.
- [43] V.L. Stolyarova, A.L. Shilov, S.I. Lopatin, V.A. Vorozhtcov, D.A. Yurchenko, N. B. Knyazyan, G.G. Manukyan, High-temperature mass spectrometric study and modeling of ceramics based on the Al₂O₃-SiO₂-ZrO₂ system, *Rapid Commun. Mass Spectrom.* 37 (2023) e9433, <https://doi.org/10.1002/RCM.9433>.
- [44] V.A. Vorozhtcov, V.L. Stolyarova, S.A. Kirillova, S.I. Lopatin, A.L. Shilov, Thermodynamic properties of quaternary systems based on hafnia: a high-temperature mass spectrometric study and modeling, *Russ. Chem. Bull.* 72 (2023) 148–157, <https://doi.org/10.1007/s11172-023-3719-z>.